Cancer Nanotechnology

RESEARCH Open Access

A novel PH1/pE27HGFK1 nanoparticles for orthotopic glioblastoma therapy

Jian zhang[2,3†], Tao Li[1†], Ling Liu[3], Zhenpu Chen[1], Li Li[1], Xiaoxuan Yao[1], Jiaxing Cheng[1], Xiaoyuan Hu[1], Jiyin Guo[1], Ruilei Li[1], Chunlei Ge[1], Eng-Ang Ling[4] and Hong Yao[1,3*]

†Jian zhang and Tao Li have contributed equally to this manuscript.

*Correspondence: yaohong20055@hotmail.com

[1] Cancer Biotherapy Center & Cancer Research Institute, Peking University Cancer Hospital Yunnan, Yunnan Cancer Hospital, The Third Affiliated Hospital of Kunming Medical University (Tumor Hospital of Yunnan Province), Kunming 650106, China
[2] Department of Respiratory Medicine, Second Affiliated Hospital of Xuzhou Medical University, Xuzhou, China
[3] Cancer Institute, Xuzhou Medical University, Xuzhou, Jiangsu Province 221002, People's Republic of China
[4] Department of Anatomy, Yong Loo Lin School of Medicine, MD10, 4 Medical Drive, Singapore 117594, Singapore

Abstract

Background: The therapeutic resistance to ionizing radiation (IR) and angiogenesis inhibitors is a great challenge for clinicians in the treatment of glioblastoma, which is associated with Hepatocyte growth factor (HGF)/MET, VEGF/VEGFR signaling pathway, and the crosstalk between them. In this study, we developed a novel recombinant fusion protein, rE27HGFK1, via HGFK1 tandem with 27 N-terminal residues of Endostatin (E27) and produced a polymeric nanoparticle formed by the co-polymer of PEGylated H1 cationic polymer (PH1) with a plasmid encoding the secreted rE27HGFK1 protein (PH1/pE27HGFK1). We further investigated the anti-tumor effects of rE27HGFK1 and PH1/pE27HGFK1 nanoparticles both in vivo and in vitro.

Methods: We expressed and purified the rE27HGFK1 protein via *E. coli*. Then, we performed cellular experiments to determine the antitumoral effects and IR radiosensitivities of the rE27HGFK1 protein in vitro. Finally, we performed animal studies to determine the tumor-targeted abilities and antitumoral activities of the polymeric nanoparticles, PH1/pE27HGFK1, in an orthotopic U118-Luc-bearing xenografted mouse model.

Results: We showed that rE27HGFK1 inhibited the proliferation and the angiogenesis and enhanced the senescence and radiosensitivity of GBM via both MET and VEFGR2 signaling mediated-p16 over-expression and the down-regulation of cyclin D1-CDK4-Rb axis activities in vitro. Next, we displayed that systemic administration of the PEGylated H1 cationic polymer (PH1) effectively delivered the reporter genes to the brain tumor of an orthotopic U118-bearing xenografted mouse model. Finally, we showed that PH1/pE27HGFK1 significantly produced antitumor effects with radiosensitivity in the orthotopic U118-Luc-bearing xenografted Blab/c mouse model through inhibiting angiogenesis and tumor cell proliferation, as well as inducing the necrosis of tumor cells in vivo.

Conclusions: The PH1/pE27HGFK1 nano-drug combined with radiotherapy can be used as a potentially effective therapeutic strategy for Glioblastoma multiforme.

Keywords: Glioblastoma, Angiogenesis, Radiosensitivity, Blood–brain barrier permeability, Cationic polymer, Gene delivery

Introduction

Glioblastoma multiforme (GBM) is a highly invasive, common, refractory primary malignant brain tumor with only a median survival time of 14.6 months and a 2-year survival rate of less than 30% (Carlsson et al. 2014), even in patients treated with surgical resection followed by chemoradiotherapies (CRT). Ionizing radiation (IR) and angiogenesis inhibitors have been the primary therapeutic modality and routine adjuvant care for patients with unresectable glioblastoma (Fletcher-Sananikone et al. 2021). However, many of them still suffer from tumor recurrence, with some patients eventually producing the inevitable progress received the anti-anagenesis treatment. Recently, many investigations have described these therapeutic resistances with Hepatocyte growth factor (HGF)/MET and VEGF/VEGFR signaling pathways (Daudigeos-Dubus et al. 2017) and the crosstalk between them (Carvalho et al. 2021; Morgan et al. 2022)

HGF/MET functions in regulating cell growth and mobility of endothelial and epithelial cells physiologically (Gao et al. 2019a, b). Its abnormal expression plays a critical role in stemness reprogramming, CRT resistance, and recurrence in GBM (Cheng and Guo 2019a; b). VEGF/VEGFR signaling pathways principally contribute to the tumor angiogenesis and tumorigenesis of GBM (Ahir et al. 2020). Bevacizumab, a humanized monoclonal antibody against VEGF, has been used to treat recurrent GBM, but it usually induces transient and inevitable progress in GMB patients (Kim et al. 2018). These unexpected responses have been attributed to the MET activation induced by the VEGF blockade. On the other hand, MET disruption increased the VEGFR2 protein stable ability in the cytoplasm, leading to the compensatory VEGFR2 and MEK signaling activation to promote tumor growth (Grojean et al. 2021; Xie et al. 2023). This suggests that simultaneous inhibition of MET and VEGFR2 may be an effective therapeutic strategy for the clinical management of GBM.

Previously, we have documented that HGFK1, the N-terminal kringle1 fragment (residues 123-210) of human HGF α-chain, was a potential radiosensitizer and angiogenesis inhibitor via targeting against MET-ATM-Chk2 axis activity (Zhang et al. 2018a, b, c). In this study, we hypothesized that a secretory fusion protein, composed of the HGFK1 linked with the 27 N-terminal residues fragment of Endostatin (E27) (Cattaneo et al. 2003; Tjin Tham Sjin et al. 2005), a predominant domain to targeting against VEGFR2 of Endostatin, might simultaneously inhibit MET and VEGFR2 and produce more potent antitumor activities for the treatment of the advanced GBM.

In the present, we have shown for the first time that the recombinant protein rE27HGFK1 inhibited the proliferation and enhanced the senescence and radiosensitivity of the U118 and U251, two cell lines of GBM, as well as repressing the angiogenesis of HUVEC cells, an endothelial cell line, by decreasing both MET and VEFGR2 signaling mediated-p16 expression and the cyclin D1-CDK4-Rb axis activities in vitro. Furthermore, to develop an effective and safe treatment for GMB in vivo, we have used a previously synthesized co-polymer PH1, consisting of the low molecular weight PEI (M.W. 600 Da) linked to β-cyclodextrin with the conjugation of polyethylene glycol (PEG, M.W. 3300 Da) and the folic acid l (Liu et al. 2018), to form a polymeric nanoparticle. We showed here that the PEGylated H1 cationic polymer (PH1) effectively delivered the reporter genes to the brain tumor of an orthotopic glioma mouse model.

Finally, we demonstrated that systemic administration of the polymeric nanoparticles, PH1/pE27HGFK1, significantly produced antitumor effects with radiosensitivity in the orthotopic U118-Luc-bearing xenografted Blab/c mouse model by inhibiting angiogenesis and proliferation of tumor cells, as well as inducing the necrosis of tumor cells in vivo.

Results

rE27HGFK1 significantly inhibits the proliferation of glioblastoma cells and the angiogenesis of endothelial cells in vitro

To study the anti-tumor and anti-angiogenic activities of E27HGFK1, we first constructed a prokaryotic expression vector of the fusion recombinant protein by use of the pTXB1 (CBD tag self-cutting expression vector) plasmid system in which a rigid AEAAAKEAAAKA-linker tandem HGFK1 and E27 was cloned. *E. coli* BL21 (DE3) was used to express the fusion protein. As shown in Supplementary Fig. 1, the rE27HGFK1 with high purity and high quality was obtained by IPTG induction, chitin affinity chromatography, and purification. After that, we determined its effects on the proliferation of U118 and U251, two GBM cell lines, via CCK-8 cell viability assay. The results showed that the cell viability of U118 and U251 cells treated by the recombinant protein (rE27HGFK1) was significantly reduced with dose-increasing. The half inhibitory concentration (IC50) of rE27HGFK1 to U118 and U251 cell lines was about 35 μg/ml and 22 μg/ml, respectively (Supplementary Fig. 2). When compared with our previously published data that the IC50 of rHGFK1 to U251 cell line is about 60 μg/ml, it indicated that the cytotoxicity on GBM cells of rE27HGFK1 was higher than that of rHGFK1. Furthermore, we determined the effects of rE27HGFK1 on the proliferation of U118 and U251 cell lines via 5-Ethynyl-2′-deoxyuridine (EdU) staining assay. As shown in Fig. 1A, the EdU-positive cells in U118 and U251 treated by single rHGFK1 and rE27HGFK1 was 2.5- and 2.2-fold lower than that of the control groups, respectively. These results indicated that similar to rHGFK1, rE27HGFK1 also inhibited the viability of GBM cells via repressing the proliferation in vitro.

We also determined the effects of these recombinant proteins on the cellular senescence of GBM via β-galactosidase staining. As shown in Fig. 1B, the proportion of β-galactosidase in U118 cells treated with rHGFK1 and rE27HGFK1 was 4.4- and 4-fold higher than that in the control group, respectively. This indicated that both rHGFK1 and rE27HGFK1 can effectively stimulate the senescence of GBM cells.

In addition, in human umbilical vein endothelial cells (HUVEC), we added the same dose of rE27 and rE27HGFK1 to explore the difference in angiogenesis inhibition. After 6 h of treatment, rE27 and rE27HGFK1 proteins significantly inhibited the angiogenic ability of HUVEC. Of these, the anti-angiogenic effect of rE27HGFK1 was more potent than that of rE27 (Fig. 1C). The above results suggest that rE27HGFK1 may exert potential antitumor activities on GBM by inhibiting tumor cell proliferation, promoting tumor cell senescence and inhibiting angiogenesis.

rE27HGFK1 inhibits the expression of MET/VEGFR2 receptor and enhances radiosensitivity

CRT resistance is a common side effect of GBM therapy, often leading to cancer recurrence. To determine whether IR combined with rE27HGFK1 would produce a more effective anti-tumor effect, we further determined the colony formation rate of different

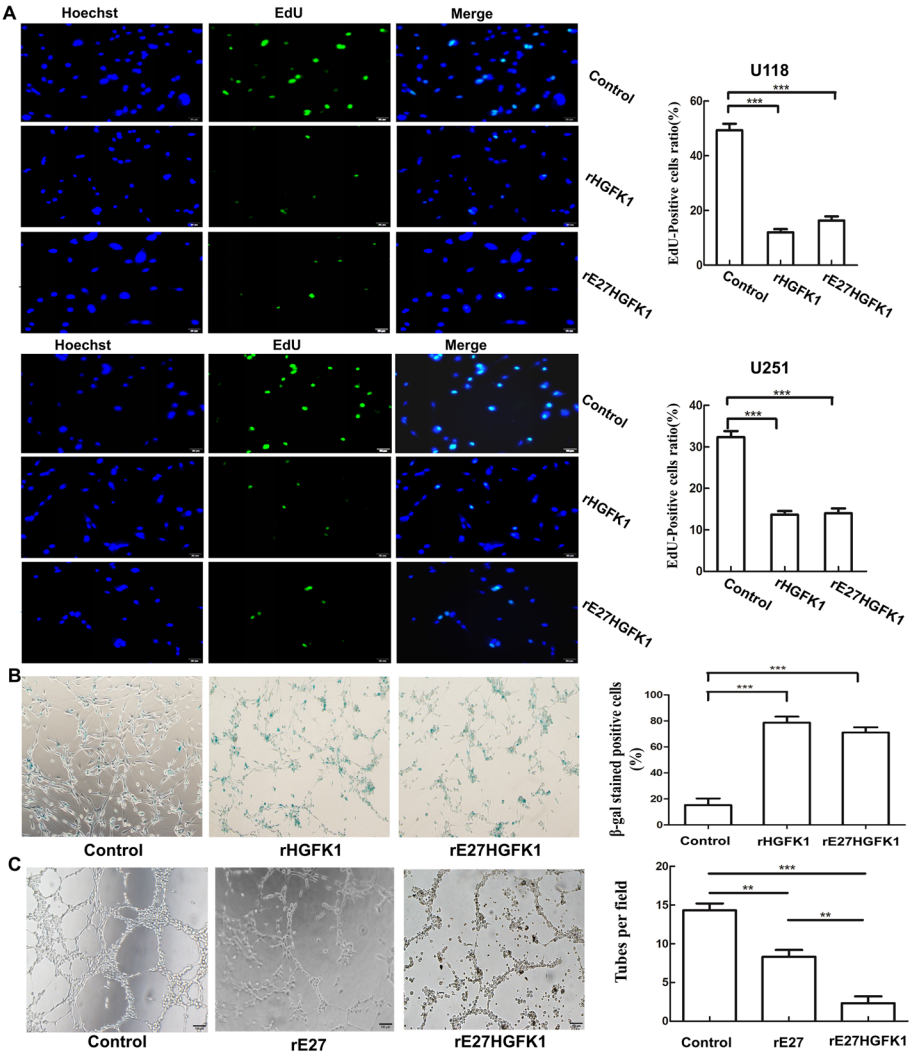

Fig. 1 The fusion protein rE27HGFK1 significantly inhibited the proliferation, angiogenesis, and colony formation of GBM. **A** The proliferation of U118 and U251 cells treated with rE27HGFK1 and rHGFK1 of 40 μg/ml for 48 h was measured by EDU (50 nM) assay. The living cells were stained with 10 μg/ml nuclear re-staining agent Hoechst33342 (100 μl/well) for 20 min. The EDU-positive cells were observed and counted in the under-fluorescence microscope (right). **B** β-galactosidase staining was used to detect the proportion of senescent U118 cells treated with rHGFK1 and rE27HGFK1 for 48 h. **C** The angiogenic ability of HUVEC cells treated with E25 or E27HGFK1 for 6 h. Five visual fields were randomly selected under a 40 × microscope to observe and calculate the number of vascular endothelial cells. (Student's *t*-test. $n = 3$, $^{*}P < 0.05$, $^{**}P < 0.01$, $^{***}P < 0.001$)

IR doses combined with rE27HGFK1. As shown in Fig. 2A, with the increase of IR dose, the colony formation of GBM cells decreased gradually, and the number of colony formation in IR combined rE27HGFK1 (10 μg) was lower than that in the same dose of single IR, this alluding that rE27HGFK1 could increase the sensitivity of GBM cells to IR.

To further investigate the IR-sensitizing effect of rE27HGFK1, we used a single-click multi-target model (MTSH model) and linear quadratic model (LQ model) to fit the survival fraction (SF) curve of U251 cells under the condition of single IR or IR combining with rE27HGFK1. As shown in Fig. 2B, C, the SF of U251 cells treated with IR combined with rE27HGFK1 was lower than that treated with IR alone. It is worth noting

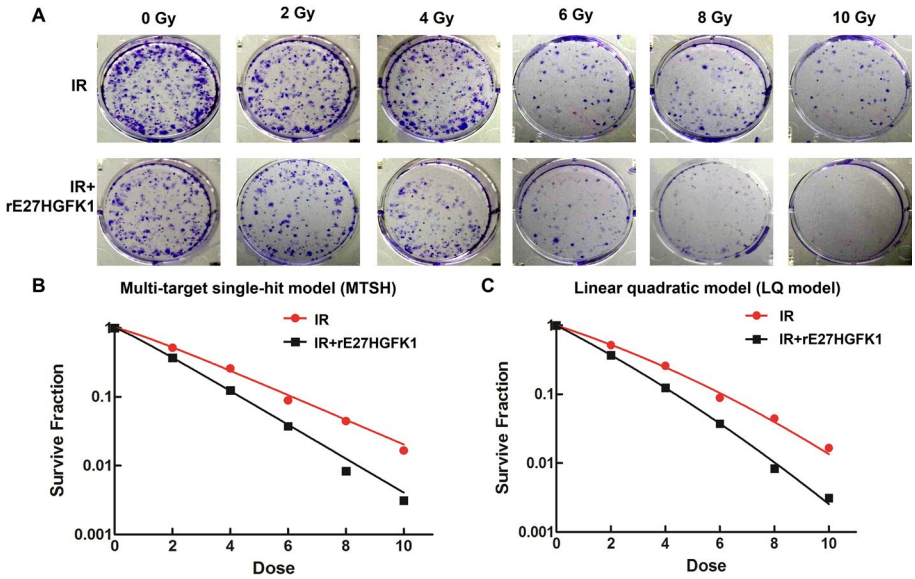

Fig. 2 rE27HGFK1 inhibits the expression of MET/VEGFR2 receptor on the surface of GBM and enhances radiosensitivity. **A** Representative images of U118 cell colony formation treated with IR alone or in combination with rE27HGFK1. B&C. The dose-U118 cell survival fraction (SF) curves were fitted by the multi-target single-hit (MTSH) model (**B**) and linear quadratic (LQ) model (**C**) after treatment with IR or IR + rE27HGFK1. SF was given by GraphPad Prism 5.0, $n = 3$, mean ± s.d

that the SF fitted by both models showed that as the IR dose increased, the addition of rE27HGFK1 reduced the SF value of GBM cells more significantly, especially when the IR was 10 grays, the SF value was decreased by more than fivefold (Table 1). In addition, in the multi-target single hit model, the sensitization enhancement ratio (SER) of the rE27HGFK1 treatment was determined to be 1.367, whereas all other radiobiological parameters, including median lethal radiation dose (D_0, Gy), the extrapolation number (N) and the quasi-threshold were reduced upon the addition of rE27HGFK1 (Table 2). Consistently, LQ model analysis showed that the cell's radiosensitivity value (α) was

Table 1 The rate of surviving fraction in two groups ($n = 3$, mean ± s.d.)

Dose (gy)	0	2	4	6	8	10
IR	1.000	0.519 ± 0.01	0.259 ± 0.02	0.889 ± 0.02	0.044 ± 0.004	0.017 ± 0.005
IR+rE27HGFK1	1.000	0.371 ± 0.02	0.125 ± 0.01	0.038 ± 0.01	0.008 ± 0.002	0.003 ± 0.002

The cell survival fraction (SF) of IR- and IR + rHGFK1-treated groups, respectively. D_0 and N represent the median lethal radiation dose (Gy) and the extrapolation number, respectively

Table 2 Comparison of radiation biological parameters between two groups (multi-target single-hit model)

Group	D_q	D_0	N	SF2	SER_{D0}
IR	0.633	2.406	1.301	0.519	1.367
IR+rE27HGFK1	0.315	1.759	1.196	0.371	

IR ionizing radiation

D_q represents the quasi-threshold that was calculated by the Equation $D_q = D_0 \times 1$ nN; SF2 represents the survival fraction (SF) for cells treated with IR at 2 Gy that can be calculated according to the equation $SF = 1 - (1 - e^{D/D0})^N$. The sensitization enhancement ratio (SER) was calculated according to the values of D_q and SF2, where SER = D_0 of the control group/D_0 of the experimental group

increased by 1.6-fold, and the parameters (α/β ratios) that increase the cell killing rate with increasing dose also significantly increased by nearly two times, compared with the single IR-treated cells (Table 3). All these data points to the fact that the addition of rE27HGFK1 reversed the radio-resistance and induced the increased radiosensitivity of GBM cells.

Systemic administration of the PEGylated H1 (PH1)/pDNA nanoparticle effectively delivers a gene into the brain tumor in an orthotopic GMB mouse model

In our previous study, we synthesized a cationic polymer (PEI-CyD-FA, named H1) (Yao et al. 2009), which was crosslinked with the low molecular weight polyethylene imine (PEI, M.W.6 Da) by β-cyclodextrin and grafted with folic acid (FA). This polymer has been shown to possess low cytotoxicity and excellent gene delivery abilities in GBM cells. To prolong the blood circulation time, we grafted a hydrophilic polymer polyethylene glycol (PEG) to PEI-CyD to form a new polymer, PEG-PEI-CyD. Further, we produced a novel Peg-late polymer (Peglated-H1, PH1) by mixing H1 with PEG-PEI-CyD at a ratio of 1:1. Cationic polymer and DNA plasmids were wrapped to form nanoparticles. We first studied the optical conditions to form the PH1/pDNA nanoparticles. As shown in Supplementary Fig. 3, the polymeric nanoparticles of PH1/pDNA formed at the 20:1 of N/P ratio showed the smallest particle size (87 ± 4.5 nm) with the Zeta potential at 6.68 ± 0.33 mV, which were also stable at physiological solution. We used these parameters to produce the PH1/pDNA polymeric nanoparticle for all subsequent experiments in this study.

In order to determine the distribution of the polymeric nanoparticles, we used in vivo imaging to screen the 6-week-old Babl/c mice at 48 h post-IP injection of H1/pLuciferase and PH1/pLuciferase nanoparticles. As shown in Supplementary Fig. 4A, the bioluminescent signals of the luciferase gene expressed aggregately in the upper abdomen, the body surface projection area of the liver, of mice treated with H1/pLuciferase polymeric nanoparticles. In contrast, the bioluminescent signals of the upper abdomen of mice treated with PH1/pLuciferase polymeric nanoparticles were significantly decreased. Remarkably, part of the bioluminescent signals was aggregated and emitted in the brain (Supplementary Fig. 4B).

Next, we constructed the eukaryotic expression vectors pE27HGFK1 and pHGFK1 (Supplementary Fig. 5A) and confirmed that they could be stably transcribed and expressed in GBM lines (Supplementary Fig. 5B). Furthermore, The pE27HGFK1 prestained with YOYO-1 (an DNA staining agent) was, respectively, encapsulated in H1 and PH1 cationic polymers, and then the blood–brain barrier permeability of H1/

Table 3 Comparison of radiation biological parameters between two groups (L-linearity quadric-model)

Group	α	β	α/β	SF2
IR	0.297	0.013	22.846	0.519
IR+rE27HGFK1	0.471	0.013	36.231	0.371

IR ionizing radiation

The radiobiological parameters of the IR− and IR+ rHGFK1-treated groups for the linear quadratic (LQ) model. $SF = e^{-\alpha D - \beta D2}$, α, β, α/β, and SF2 were given by GraphPad Prism 5.0 based on the curve of the LQ model previously

pE27HGFK1-YOYO-1 and PH1/pE27HGFK1-YOYO-1 nanoparticles were determined by IP injection. As shown in Fig. 3A, B, there was an obvious accumulation of YOYO-1 fluorescence in the brain of mice treated with PH1/pE27HGFK1-YOYO-1, but no YOYO-1 signals were detected in the brain of mice treated with H1/YOYO-1-pHGFK1. These results indicate that compared with H1/pDNA nanoparticles, PH1/PDNA nanoparticles can obviate the trapping by the liver and extend the blood circulation time. Therefore, PH1 should be an effective gene carrier polymer for the gene therapy of GBM.

To further explore whether PH1/pDNA nanoparticles can target the tumor of GBM, we established an orthotopic U118-Luc-bearing (stably expressed luciferase gene) xenografted nude Blab/c mouse model. PH1/YOYO-1-pE27HGFK1, PH1/pEGFP nanoparticles were IP injected into U118-Luc-bearing mice to detect their targeting to GBM. As shown in Fig. 3C–E, 72 h after intraperitoneal (IP) injection of these polymer

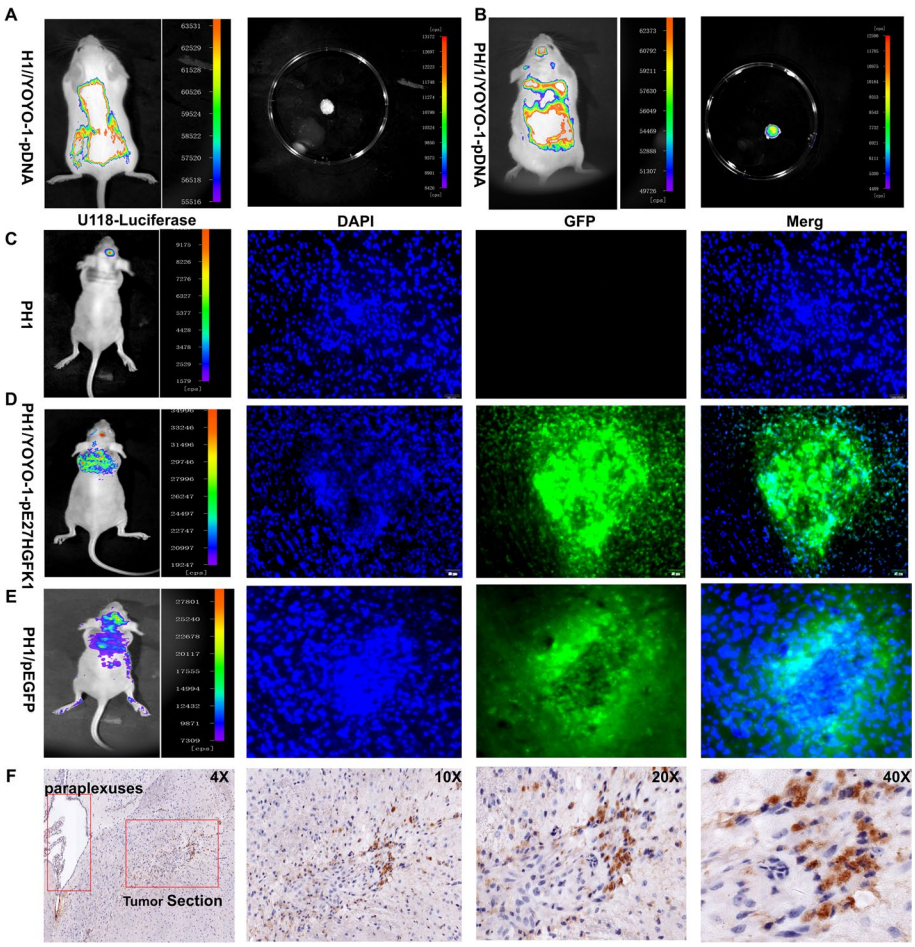

Fig. 3 Identification of blood–brain barrier (BBB) permeability and brain GBM tumor targeting of PH1/pE27HGFK1 nanocomposites. **A**, **B** The distribution of YOYO-1 labeled pDNA (pE27HGFK1) in Balb/c mice observed at 24 and 72 h after intraperitoneally injected with H1/YOYO-1-pDNA and PH1/YOYO-1-pDNA. **C**–**E** Distribution of PH1 (**C**), PH1/YOYO-1-pHGFK1 (**D**), PH1/pEGFP (**E**) nanoparticles in the GBM U118-Luc-bearing orthotopic xenografted nude Blab/c mouse model after IP injection. Immunohistochemical study of PH1 (**C**), PH1/YOYO-1-pHGFK1 (**D**), PH1/pEGFP (**E**) nanoparticles in frozen sections of brain tissue of U118-Luc-bearing mice. **F** Immunohistochemical staining showed that the PH1/ pEGFP nanoparticles had blatant tumor targeting, and EGFP protein was highly expressed in tumor tissue

nanoparticles, the YOYO-1 fluorescence distribution of PH1/YOYO-1-pE27HGFK1 (Fig. 3D) and the GFP signal of PH1/pEGFP (Fig. 3E) both highly corresponded to the bioluminescence signal of U118-luciferase in the orthotopic xenograft mice, compared to the PH1 control group (Fig. 3C).

Subsequent frozen sections of brain tissue showed that the green signals of YOYO-1-pE27HGFK1 and GFP fluorescence were both concentrated in the core area of the tumor tissue (Fig. 3C–E). In addition, we confirmed the expression and localization of GFP protein in brain tumors after treatment with PH1/pEGFP nanoparticles using immunohistochemical staining. As shown in Fig. 3F, the GFP-positive cells were observed in choroid plexus epithelial cells in PH1/pEGFP-treated mice. The results show that PH1/pDNA nanoparticles successfully deliver therapeutic genes into brain tumor masses of GBM, thus, PH1/pDNA nanoparticles are suitable for GMB gene therapy.

PH1/pE27HGFK1 polyplexes enhance the radiosensitivity of the GBM in vivo

To determine the anti-tumor effect of PH1/pE27HGFK1 nanoparticles combined with radiotherapy in orthotopic U118-Luc-bearing xenografted mice. The tumor burden indicators, such as tumor size and survival time of the orthotopic U118-Luc-bearing xenograft mice on the 7th and 14th day after all the above treatments, were observed and counted. Our results showed that there was no significant difference in brain tumor fluorescence count between different treatment groups on the 7th day (Supplementary Fig. 6). After 14 days, the mean region of interest (ROI) in U118-bearing mice treated with IR, PH1/pHGFK1 and PH1/pE27HGFK1 group was 543,252, 587,693, 536,749 respectively, which were onefold lower than that of the control group (815,439) and PH1/pEGFP-treated (863,321) (Fig. 4A, B). When radiotherapy was combined, the ROI means of IR + PH1/pHGFK1 and IR + PH1/pE27HGFK1 in U118-bearing mice were 254,679 and 215,437, respectively, which were lower than that of IR (543,252), PH1/pHGFK1 (587,693) or PH1/pE27HGFK (536,749) single-treated, predominantly the ROI of the PH1/pE27HGFK combined radiotherapy group was the lowest among all treatment groups (215,437) (Fig. 4A, B). These data indicate that PH1/pE27HGFK alone has an excellent antigenic effect on glioma, and its combined radiotherapy can increase radiotherapy sensitivity and achieve a more powerful anti-tumor effect.

In terms of survival time, the total survival time of the IR + PH1/pE27HGFK1 treatment group was the longest, reaching 52 days, and 50% of mice in the IR + PH1/pE27HGFK1 and IR + PH1/pHGFK1 treatment groups survived more than 45 days, which was better than that of the single treatment group (Fig. 4C). The above data fully reflect the excellent anti-tumor effect of radiotherapy combined with PH1/pE27HGFK1 nanoparticles in GBM.

These data suggested that systemic administration of PH1/pE27HGFK1 nanoparticles could effectively inhibit tumor growth and prolong the survival of the tumor-bearing mice in the orthotopic U118- Luc-bearing xenografted mouse model.

PH1/pE27HGFK1 polymeric nanoparticles export antitumor and radiosensitivity activities via inhibition of tumor proliferation and anti-angiogenesis in vivo

To investigate the potential mechanism of PH1/pE27HGFK1 inhibition on tumor morphology/pathological appearance, GBM proliferation, apoptosis, and angiogenesis

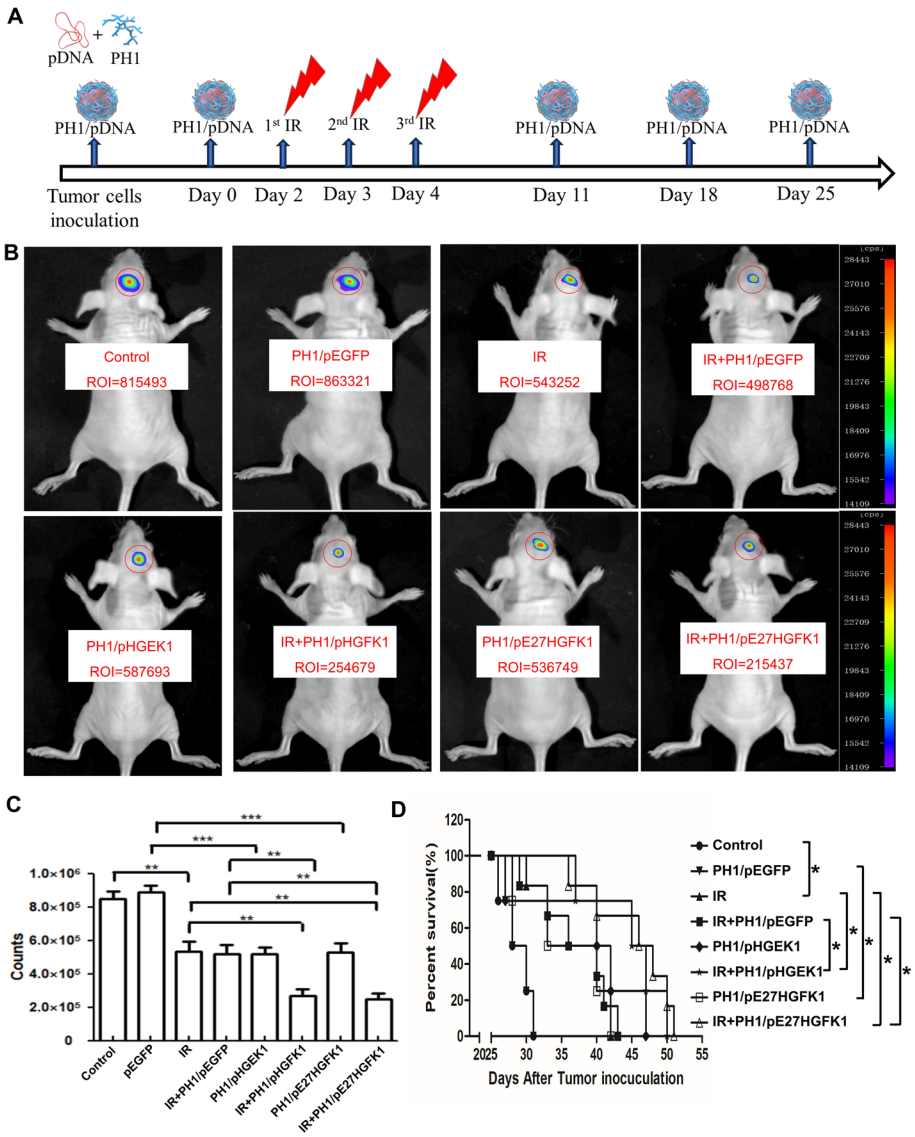

Fig. 4 The anti-tumoral and radiosensitization functions of pH1/pE27HGFK1 nanoparticles in the orthotopic U118-Luc-bearing xenografted nude mouse model. **A** A schematic diagram illustrated the therapeutic schedule according to the materials and methods. **B** After being treated with PH1/pE27HGFK1, PH1/pHGFK1, PH1/pE27HGFK1 + IR, PH1/pHGFK1 + IR, PH1/pEGFP, PH1/pEGFP + IR, IR and 5% glucose for 14 days, the tumor fluorescence density and counting values were calculated by in vivo optical imaging system. **C** Statistics and analysis of tumor fluorescence densitometer after 14 days of treatment in different experimental groups. **D** Survival curve of U118-Luc-bearing mice in different treatment groups

in vivo, we observed the pathological feature by histochemistry and determined the expression of Ki67, a proliferation biomarker, and the micro-vessel density (MVD) in tumor tissue by immunohistochemistry.

As shown in Supplementary Fig. 7, by hematoxylin–eosin (HE) staining, there was uneven staining and obvious contrast in staining intensity. Strong staining areas were observed in the tumor tissue of mice treated with the control reagents at two weeks post-treatment. However, the strong staining areas of tumor tissue were significantly reduced in mice treated with IR single, PH1/pHGFK1 single, or PH1/pE27HGFK1 single groups,

respectively. In the tumor tissue of mice treated with IR + PH1/pHGFK1 or IR + PH1/pE27HGFK1, respectively, the strong staining areas had almost disappeared. Suggesting that IR single, PH1/pHGFK1 single, PH1/pE27HGFK1 single, IR + PH1/pHGFK1 and IR + PH1/pE27HGFK1 treatments had attenuated the activities of tumor cells in the orthotopic U118-Luc-bearing xenografted mouse model.

Furthermore, we showed that the staining of the proliferation biomarker Ki67 in tumor tissue of mice treated with IR alone, IR + PH1/pEGFP, PH1/pHGFK1, and PH1/pE27HGFK1 was reduced by 2/3 but that in the groups treated with IR + PH1/pHGFK1 or IR + PH1/pE27HGFK1 was reduced by 1/3 of that in control or PH1/pEGFP alone-treated groups, respectively (Fig. 5A, C). In comparison with the control or PH1/pEGFP alone-treated groups, the apoptotic biomarker Tunnel staining in tumor tissues of mice treated by IR alone or IR + PH1/pEGFP treated groups were a two-fold increase, that of PH1/pHGFK1 alone treatment was a three-fold increase, and that of PH1/pE27HGFK1 alone, IR + PH1/pHGFK1 or IR + PH1/pE27HGFK1 treatments were four-fold increase (Fig. 5B, C). These data indicated that both PH1/pHGFK1 alone and PH1/pE27HGFK1 alone can inhibit proliferation, induce apoptosis, and systemically enhance the radiosensitivity of glioblastoma cells in vivo. Among them, PH1/pE27HGFK1 treatment exhibits the highest pro-apoptosis ability.

In addition, we also determined the micro-vessel density (MVD) of tumor tissues treated with various reagents using CD31 immunohistochemical staining. As shown in Fig. 5D, E, the MVD of mice treated by PH1/pHGFK1 alone was reduced by 1/3 of the control, but that of mice given PH1/pE27HGFK1 alone was reduced by 2/3 that of the control. This indicated that the anti-angiogenic ability of PH1/pE27HGFK1 was more than that of PH1/pHGFK1.

rE27HGFK1 exerts anti-tumor effects by inhibiting both MET and VEGFR2 pathways, upregulating P16, and decreasing cyclin D1-CDK4-Rb *axis* activities

Our previous studies have reported that HGFK1 plays an anti-tumor and radio-sensitizing effect by inhibiting and reversing the activity of IR-induced MET and ATM-Chk2 axes (Zhang et al. 2018b). To explore the potential molecular mechanism of the anti-tumor effects of rE27HGFK1, we first determined the protein expression level of Met and VEGFR2, the proposed targeted receptors of rE27HGFK1, in U118 cells treated by IR single, rE27HGFK1 single, and their combining treatments in vitro.

As shown in Fig. 6A, B, rE27HGFK1 treatment alone obviously down-regulated the protein expression of both Met and VEGFR2 (Line 3). Conversely, IR single treatment slightly increased the protein expression level of MET and VEGFR2 (Fig. 6A, B, Line 2). rE27HGFK1 + IR reversed the enhancement of MET and VEGFR2 protein expression induced by IR alone (Fig. 6A, B, Line 4). These data indicate that rE27HGFK1 produced the antitumor effects mainly via inhibition of the activities of both MET and VEGFR2 signaling pathways, which also contribute to its IR-enhancing sensitivities.

In addition, as mentioned above, we first showed that both rHGFK1 and rE27HGFK1 can induce the senescence of glioblastoma cells in vitro, but the potential molecular mechanisms remain to be clarified. As shown in Fig. 6C, D, compared to that of the control, the expression of pro-aging marker p16 in rHGFK1- and rE27HGFK1-treatments was 1.2- and 2.6-fold increased, respectively. However, the levels of the cyclind1,

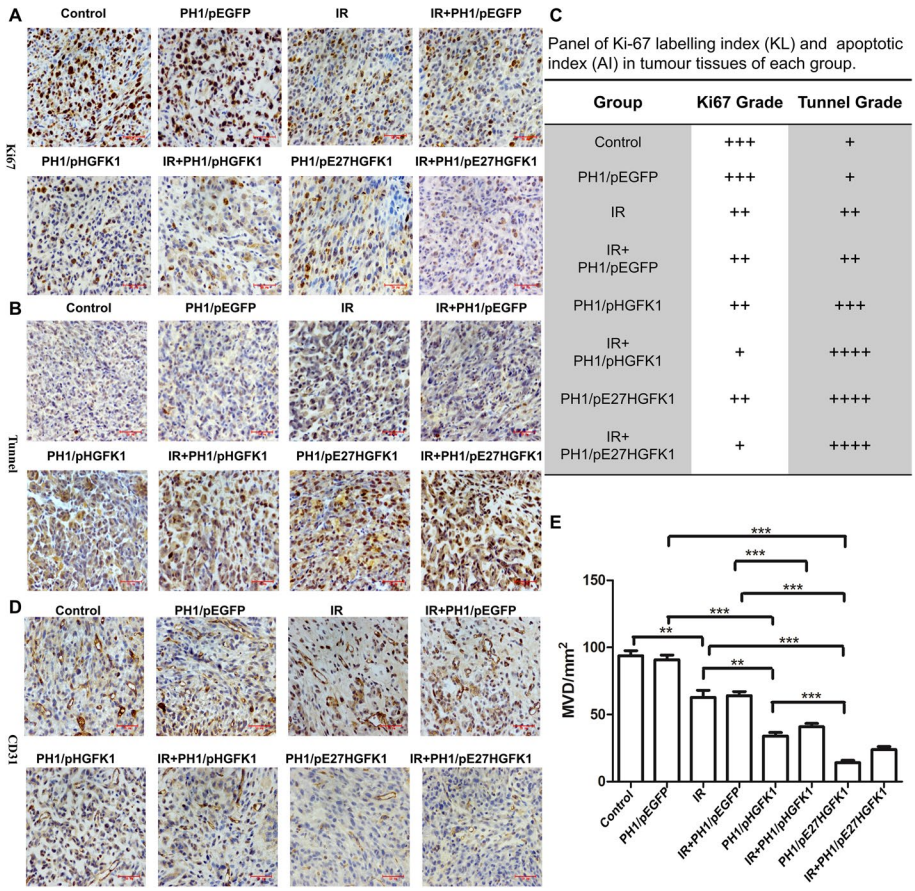

Fig. 5 Immunohistochemical study on the inhibition of tumor proliferation, apoptosis, and angiogenesis in U118-luc-bearing mice by PH1/pE27HGFK1 combined with radiotherapy. **A** Ki67 immunohistochemical staining and scoring of paraffin sections of brain tissue were performed 14 days after different treatments. **B** Tunel immunohistochemical staining and scoring. **C** Panel of Ki-67 labelling index (KL) and apoptotic index (AI) in tumor tissues of each group. **D** Representative image and score of CD31 immunohistochemical staining of microvessel density (MVD). **E** Statistics of MVD in brain tissue sections of different treatment groups

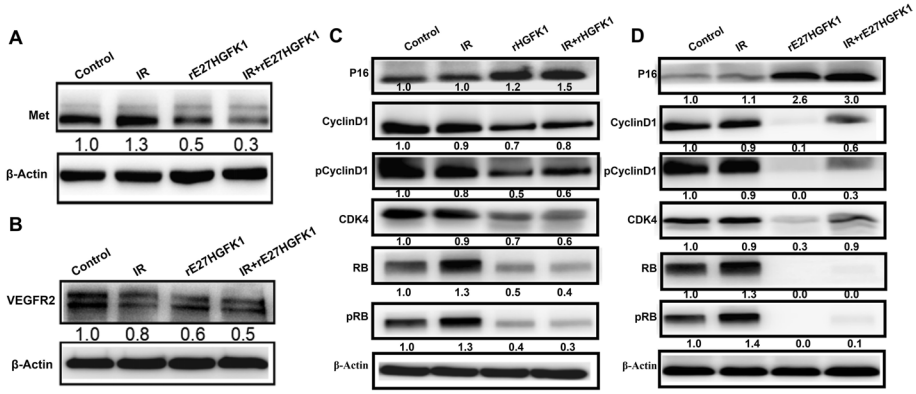

Fig. 6 Western blotting confirmed the anti-tumor molecular mechanism of rHGFK1. **A**, **B** Western blot was used to detect the expression of MET and the VEGFR2 receptor in U118 cells treated with rE27HGFK1, IR, and their combination. **C**, **D** The effects of rHGFK1 and rE27HGFK1 alone or in combination with radiotherapy on p16 and cyclin D1-CDK4-Rb axis activities related to cell cycle arrest and senescence in U118

phosphorylation of cyclind1, cyclin-dependent protein 4 (CDK4), Rb, and phosphorylation of Rb in HGFK1- or rE27HGFK1- treated cells were reduced to 0.7-, 0.5-, 0.7-, 0.5-, 0.4- or 0.1-, 0.0-, 0.3-, 0.0-, 0.0-fold of that in control, respectively. These results suggest that rHGFK1 and rE27HGFK1 can upregulate the p16 expression and downregulate the cyclin D1-CDK4-Rb axis activities, resulting in the G1 phase cell cycle arrest and cell senescence of glioblastoma cells.

Of note, when we compared with the control group, the Rb protein expression and its phosphorylation level in glioblastoma cells treated by IR were increased by 1.3- and 1.3-fold, but with rHGFK1- and rE27HGFK1-treatments, they were reduced to 0.5 and 0, respectively. As expected, both IR + rHGFK1- and IR + rE27HGFK1-treatment reduced the Rb protein expression and its phosphorylation level in glioblastoma cells. The results indicated that rHGFK1 and rE27HGFK1 inhibited the RB pathway, which contributed to the radiosensitivity ability of glioblastoma cells.

Discussion

Glioblastoma remains a refractory tumor for clinical because of the tumor heterogeneity and the resistance to antiangiogenetic and radiotherapy (Alifieris and Trafalis 2015; Gatto et al. 2022). Gene therapy is deemed to be a promising treatment for the treatment of GBM. However, due to the existence of BBB (Van Tellingen et al. 2015), developing a gene therapy strategy depends on a safe, effective, and tumor-targeted gene carrier for GBM treatment (Alphandéry 2020). We previously synthesized a cationic polymer (PEI-CyD-FA, named H1) with low toxicity, high efficiency, and folic acid ligand targeting. However, this polymer is quickly captured by the hepatic reticuloendothelial system, and it cannot achieve blood–brain barrier penetration.

In this study, we grafted a hydrophilic polymer PEG (P.W. 3300) to H1 and showed that the fluorescence signals of the PH1/YOYO1-E27HGFK1, PH1/pluciferase, and PH1/pEGFP nanoparticles all could accumulate and display in the tumor mass of the mouse brain in an orthotopic glioblastoma xenografted mice model (Fig. 3). The green fluorescence of YOYO1-labeled PH1/YOYO1-E27HGFK1 nanoparticles was aggregated in the tumor mass, but the green fluorescence of GFP expressed by PH1/pEGFP nanoparticles was mainly distributed around the tumor mass. The differential localization may be attributed to the declined cellular activities in the control of the tumor mass as compared to that of the periphery tumor cells because YOYO1 is an organic dye that can directly emit green fluorescence under light excitation. On the other hand, the green fluorescence produced by the plasmid of the EGFP gene requires the transcription and expression of the GFP protein in a living cell with high cellular activities.

Interestingly, the GFP staining in the paraffin sections of the mouse brain performed by systemic administration of the PH1/pEGFP nanoparticles showed that the EGFP expression was detectable in the area near the lateral ventricles. Moreover, it appears to extend into the tumor mass. The PH1/pEGFP nanoparticles administrated intraperitoneally might have gained intimate access to the brain parenchyma via systemic circulation. In addition, the possibility that the nanoparticles were first ingested by blood monocytes that migrated into the brain and transformed into the microglial cells should be considered. Activated microglia might have been home in the tumor tissue by chemokine induction, which forms a principal cellular constituent of GBM. In any event,

we have shown unequivocally that the PH1 cationic polymer can effectively deliver the therapeutic gene to the tumor mass in an orthotopic glioblastoma xenografted mouse model (Tsujimoto et al. 2021a, b).

Radiation resistance remains the main challenge in glioblastoma therapy, and improving radiosensitivity has become a cutting-edge topic for the treatment of GBM (Li et al. 2022). Our previous studies have shown that HGFK1 can bind to MET receptors on the surface of GBM and inhibit its phosphorylation activity; this down-regulates stem-related Wnt/β-catenin and Notch1 pathways and results in increasing the radiosensitivity of GBM. In this study, we produced the first fused protein-E27HGFK1, whose activities of the proliferation inhibition and promotion of the senescence to glioblastoma cells were similar to that of rHGFK1, but whose anti-angiogenesis ability was significantly higher than that of rHGFK1. In the latter, it may be attributed to the additional blocking ability of E27HGFK1 to the VEGF/VEGFR2 signaling in vitro (Figs. 1, 2).

Furthermore, we showed that the systemic administration of PH1/pE27HGFK1 nanoparticles significantly inhibited tumor growth, extended the survival of the orthotopic xenografted glioma mice, and enhanced the antitumor activities of IR in vivo. All this should be attributed to the proliferation inhibition, pro-apoptosis, and anti-angiogenesis abilities of rE27HGFK1 to the glioma tumor (Figs. 4, 5). Our mechanism experiments further confirmed that rE27HGFK1 can double-target to MET and VEGFR2 (Figs. 6A, B, 7), and inhibit the proliferation and anti-angiogenesis of GBM cells. In addition, rE27HGFK can reverse the senescence and cell cycle arrest of radiation-tolerant GBM cells by up-regulating P16 and inhibiting the cyclinD1-CDK4-Rb axis (Figs. 6C, D, 7). Through this noted approach, more robust radio sensitization, pro-apoptosis and antitumor effects were achieved. Arising from this, therefore, it can be confidently concluded that PH1/pE27HGFK1 is a potential therapeutic agent for glioblastoma.

Materials and methods

Cell culture and antibodies

GBM cell lines U118 and U251 were obtained from the cell bank of the Chinese Academy of Science (Shanghai, China) and were all cultured in DMEM (high glucose) medium supplemented with 10% fetal bovine serum (FBS), 100 IU/ml penicillin and streptomycin. Human umbilical vein endothelial cells HUVEC were obtained from ATCC (Manassas, VA, USA) and cultured in EGM-2 medium supplemented with 100 μg/ml heparin, 50 μg/ml ECGS, and 10% FBS. All the cultures were maintained in a humidified incubator with 5% CO_2 at 37 ℃. All antibodies, including anti-β-actin (Cat. MAB8969), anti-MET (Cat. MAB3582), anti-VEGFR2 (Cat. MAB3571), anti-CyclinD1 (Cat. AF4196), anti-pCyclinD1 (Cat. ab62151) anti-CDK4 (Cat. AF5254), anti-RB (Cat. MAB6495), anti-pRB (Cat. 9307), anti-CD31 (Cat. AF806), anti-ki67 (Cat. AF7617) were purchased from Cell Signaling Technology R&D Systems, unless otherwise specified. YOYO-1 dye was purchased from Invitrogen (Carlsbad, CA, USA).

Prokaryotic expression and purification of rE27HGFK1, rHGFK1

Prokaryotic CBD tag self-cutting expression vector pTXB1 was purchased from Bio Vector NTCC (Hosseini et al. 2020). For the E27HGFK1 protein sequence, a rigid linker AEAAAKEAAAKA was used to connect E27

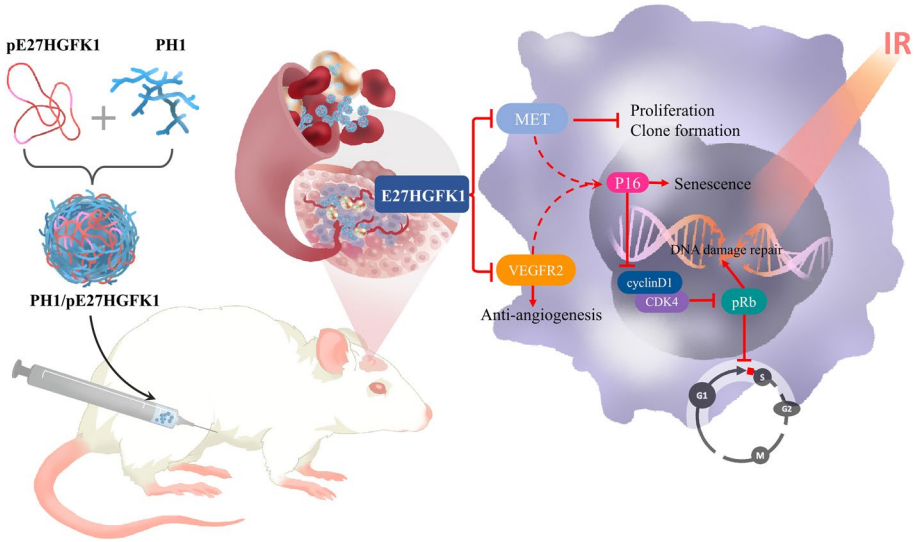

Fig. 7 Schematic diagram of the mechanism of PH1/pE27HGFK1 nanoparticles in the treatment of orthotopic GBM-bearing xenografted nude Blab/c mouse model. Intraperitoneal injection of pH1/pE27HGFK1 nanoparticles may circulate through the systemic blood circulation or be ingested by blood monocytes, which then migrate to the brain. Subsequently, the expressed E27HGFK1 targets both MET and VEGFR2, leading to inhibition of proliferation and anti-angiogenesis. It also indirectly upregulates p16 to promote senescence while inhibiting the cell cycle arrest mediated by the cyclinD1-CDK4-Rb axis. Ultimately, the action of E27HGFK1 results in the upregulation of p16 and the downregulation of pRb (the upregulation of which can resist DNA damage caused by ionizing radiation, IR), disrupting the DNA damage repair capability of pRb. Therefore, pH1/pE27HGFK1 nanoparticles enhance the sensitivity of glioblastoma multiforme (GBM) to IR, and their combination with radiotherapy shows a promising synergistic anti-tumor effect

(HSHRDFQPVLHLVALNSPLSGGMRGIR) and HGFK1 (residues 128-206 in HGF). Then, the gene fragment encoding the E27HGFK1, HGFK1 was sub-cloned into NdeI and NsiI of prokaryotic expression vector pTXB1 and expressed in *E. coli* BL21 (DE3) through inducement by IPTG. The recombinant proteins rE27HGFK1 and rHGFK1 were purified using chitin affinity beads (Buffer 20 mM Tris–HCl PH:8.5, 0.5 M NaCl, NEB #S6651) and then cleaved using 50 mM dithiothreitol (DTT) according to the manufacturer's instructions (Gao et al. 2019a; Lamer et al. 2022). The purity and concentration of rE27HGFK1 and rHGFK1 were, respectively analyzed with SDS-PAGE and a BCA protein concentration kit (Beyotime, Nanjing, China).

Construction of prokaryotic and eukaryotic expression plasmid

A CpG-free plasmid-encoding firefly luciferase (pORF-Luc) was purchased from In vivo Gene (San Diego, CA, 92121, USA). The cDNAs fragments containing IgK leader and the GFP, E27HGFK1, HGFK1 were subcloned into the pORF-Luc plasmid backbone by KasI and NheI to generate pORF-GFP (pGFP), pORF-HGFK1(pHGFK1) and pORF-E27HGFK1(pE27HGFK1), respectively. The plasmids were transformed separately into competent DH5α cells, propagated in LB broth supplemented with 100 μg/ml ampicillin, and purified with PureLink™ Hipure Plasmid Maxiprep kit (Invitrogen, Carlsbad, CA, USA). The quantity and quality of the purified plasmid DNA were assessed by measuring its optical density at 260 and 280 nm.

Cell proliferation assay

The effects of rE27HGFK1 on U118 and U251 cell proliferation were measured with a CCK-8 assay kit (VICMED, China) and EdU-based assay. The U118 and U251 cells in the logarithmic growth phase were seeded on 96-well plates at a density of 3000 cells per well in a 200 μl culture medium and allowed to adhere overnight. Subsequently, the cells were incubated with rE27HGFK1 at increasing concentrations dissolved (5 μg/ml, 10 μg/ml, 20 μg/ml, 40 μg/ml, 60 μg/ml, 80 μg/ml) in DMEM medium supplemented with 2% FBS for 48 h. The 10 μl CCK-8 dye was added and incubated for a further 2 h. The absorbance was finally determined at 450 nm using a microplate reader (Bio-Tek Instruments, Winooski, USA).

For EdU-Based Assay, U118 and U251 cells (3×10^3 cells per well) were cultured in 96 well plates in triplicate and treated with 40 μg/ml rE27HGFK1 and rHGFK1 for 48 h. Then, the cells were incubated with 50 nM's EdU at 37 ℃ for another 2 h. The cells were fixed with 4% formaldehyde at room temperature for 15 min and treated with 0.5%TritonX-100 at room temperature for 20 min to permeate the cells. After washing with PBS three times, the cells were incubated with 100ul Click-iT reaction mixture for 30 min. DNA was stained with 10 μg/ml Hoechst33342 Staining Dye Solution (100 μl/well, Thermo Scientific™) for 20 min and observed and photographed with a fluorescence microscope. Five images were randomly selected from each sample group, and the EDU-positive cells were observed and counted.

Tube formation assay

96-well plates were coated with 50 μl Matrigel (Corning) and incubated at 37 °C for 30 min. After being conducted by 30 μg/ml MOBs, exosomes for 24 h, 50 μl of HUVEC cells suspension (4×10^5/ml) was seeded in Matrigel-coated 96-well plates and incubated under 5% CO_2, 37 °C and humidified incubator for 6 h. Each experiment was conducted in triplicate. After incubation, the formation of tube-like structures was photographed using phase contrast microscopy and analyzed using Image J software.

Radiation treatment in vitro

U118 and U251 cells were seeded in 6-well plates and incubated for eight hours. After adherence, cells were treated in a Varian 23 EX Clinic linear accelerator by vertical radiation with a rack rotation angle of 180°, a dosage rate of 10 Gy min^{-1}, a source-skin distance of SSD = 100 cm, and an exposure field of 15 cm × 15cm. The bottom of the plate was covered with tissue infilling measuring 1.5 cm in height, and the same dose of radiation was received.

Colony formation assay

Colony formation dose-U118 cell survival fraction (SF) fit models were analyzed according to our previously described method (Gao et al. 2019b). Briefly, U118 and U251 cells growing in the logarithmic phase were seeded in 6-well plates. After adherence, cells were treated with rHGFK1 (10 mg/ml) in 1 ml of fresh media for 24 h, followed by radiation (0, 2, 4, 6, 8, and 10 Gy) and media change. After incubation for 14 days, the number

of colonies was counted under a microscope at low magnification. The dose-U118 cell survival fraction (SF) was fitted by GraphPad Prism 5.0, according to the multi-target single-hit (MTSH) model and linear quadratic (LQ) model. n = 3, mean ± s.d.

Preparation and characterization of PH1/pDNA nanoparticles

H1 and PH1 were synthesized according to our previously described method (Gao et al. 2019b; Zhang et al. 2018a). For PH1/pDNA nanoparticles preparation, PH1 and pDNA were vortexed in an equal volume of 5% glucose solution at different N/P ratios (where 'N' is the amount of nitrogen in PEI and 'P' is the amount of phosphate in 1 μg of DNA). The polyplexes were stabilized for 20 min at room temperature. Then, the PH1/pHGFK1 nanoparticles were freeze-dried and resuspended in deionized water prior to transfection and injection. The particle size and zeta potential of nanoparticles were measured by a Zeta potential/Particle sizing system (Nicomp 380 ZLS, USA). The in vivo distribution experiments of nanoparticles, including PH1/YOYO-1-pDNA, PH1/pGFP, and PH1/pLuciferase, were carried out with the in vivo optical imaging systems (Berthold Technologies, Germany) at the indicated time points.

Western blot assay

Serum-starved U118 cells were treated with PBS, IR (10 Gy), rHGFK1 (40 mg), rE27HGFK1 (40 mg) or in combination for 48 h. The cells were then collected, rinsed in ice-cold PBS, and lysed in a lysis buffer containing protease inhibitors. Denatured protein was separated by 10% SDS polyacrylamide gel and transferred onto a PVDF membrane (Millipore, Billerica, MA, USA). After blocking with 5% BSA in TBS-Tween 20 (0.05%, v/v), the membrane was incubated overnight at 4 ℃ with the primary antibodies: anti-β-actin, anti-Met, anti-VEGFR2, anti-CyclinD1, anti-pCyclinD1, anti-CDK4, anti-RB, anti-pRB. After washing with TBST, the membrane was incubated with HRP-conjugated anti-rabbit or anti-mouse secondary antibody for one hour at room temperature. Following several washes, peroxidase activity was visualized with an Immobilon Western HRP kit (Millipore).

U118-Luc-bearing orthotopic xenografted mouse model

All animal studies were approved by the Animal Experimental Ethics Committees of KunMing Medical University. Balb/c nude mice (4–6 weeks old) were purchased from Beijing Vital River Laboratory Animal Technology (Beijing, China) and maintained at KunMing Medical University Animal Center. According to our previous study (Zhang et al. 2018a), Blab/c mice were performed by intracranial microinjection of logarithmic phase U118-Luc GBM (1×10^7 cells) to establish a U118-Luc-bearing orthotopic brain orthotopic xenograft mouse model. The in vivo optical imaging system was used to perform Luciferase fluorescence measurement. When the fluorescence amount reached 50,000, the U118-Luc-bearing mice were randomly divided into eight groups (six mice of each group) on day 7 post-tumor cells inoculation, which was treated by solution control (5% glucose), PH1/pEGFP, PH1/pHGFK1, PH1/pE27HGFK1, IR, IR + PH1/pEGFP, IR + PH1/pHGFK1, IR + PH1/pE27HGFK1, respectively. The prepared nanoparticles were injected into mice via intraperitoneal (IP) injection. The combination with the radiotherapy procedure was followed in our previous study (Zhang et al. 2018a). Briefly,

on the day of randomization (day 0), all nanoparticles (50 mg per mouse) or PBS, 5% glucose were administered by IP injection. On Day 2, 3 and 4, IR was carried out at a dose of 10 Gy for three consecutive days. To avoid damage to important organs, mice were shielded with a lead box when exposed to radiation. At the end of IR treatment, nanoparticles were administered weekly over the next 3 weeks. The survival status of tumor-bearing mice was monitored daily. Tumor size was observed on days 7 and 14. The number of mice in each treatment group was no less than 5 and the number of plasmids used in this article was 25 μg. All statistical results are guaranteed to contain complete data of more than three mice.

Immunohistochemistry (IHC) and HE staining

Immunohistochemistry (IHC) and HE staining were performed according to our previously described method (Zhang et al. 2018a). Briefly, after two weeks of treatment in different treatment groups, brain tumor-bearing mice were euthanized, and orthotopic xenograft tumors were removed, fixed with 10% neutral buffered formalin, embedded in paraffin, and cut into 4 μm thick sections. After deparaffinization, rehydration, and boiling in 10 mM sodium citrate (pH 6.0) for 15 min, 3% H_2O_2 was used to block endogenous peroxidase activity. After blocking nonspecific antigens, the tumor sections were incubated with antibodies anti-CD133, anti-GFP, or anti-Ki67 overnight at 4 ℃, respectively. Following incubation with HRP-labeled secondary antibody (Beyotime, Nanjing, China) at room temperature for 30 min, the tumor sections were stained by DAB. Tissue sections were observed under a microscope, at least three to five fields per section were analyzed, and positively stained cells were counted using Image-Pro Plus 7.0 (Media Cybernetics, Inc., USA). For HE staining, the mouse brain tissues were also sectioned into 4 μm thick and stained using a hematoxylin and eosin staining kit (Beyotime, Shanghai, China) according to the manufacturer's protocols. Tissue sections were observed under a microscope, and at least three fields per section were analyzed.

Statistical analysis

The in vitro experiments were repeated at least three times, and the results were presented as mean ± standard deviation (SD). A two-tailed student's t-test was performed to determine the statistical significance of differences between groups. Multiple comparisons were performed using one-way ANOVA. Survival analysis of tumor-bearing mice was performed with the Kaplan–Meier method. All the data was analyzed with GraphPad Prism 5.0 (GraphPad Software, Inc., USA), and $p < 0.05$ was considered a significant difference.

Abbreviations

HGF	Hepatocyte growth factor
CRT	Chemoradiotherapy
E27	27 N-terminal residues of endostatin
BBB	Blood–brain barrier
HUVEC	Human umbilical vein endothelial cells
IR	Ionizing radiation
SF	Survival fraction
MTSH	Multi-target single-hit model
LQ	Linear quadratic model
PEG	Polyethylene glycol
H1	PEI-CyD-FA

PEI Polyethylene imine
PH1 PEG grafted H1
MVD Micro-vessel density

Supplementary Information

The online version contains supplementary material available at https://doi.org/10.1186/s12645-024-00267-1.

Supplementary Material 1.

Author contributions

Hong Yao, Eng-Ang, Ling, and Ling Liu conceived and designed the study. Jian Zhang mainly completed the experimental content of this study. Li Tao sorted out all the experimental results, wrote the manuscript, prepared all the charts, and was responsible for the delivery and follow-up work of the article. Li Li, Xiaoxuan Yao, Jiaxing Chen, Xiaoyuan Hu, Zhenpu Chen, Jiyin Guo, Ruilei Li, and Chunlei Ge assisted in the completion of experiments involving animal, immunohistochemistry, molecular cloning, protein expression purification and other studies.

Funding

The work was financially supported by the National Natural Science Foundation of China (Grant Numbers 82350117, 82160476, 32360046, 82260462, 82204314), the Joint Special Funds for the Department of Science and Technology of Yunnan Province-Kunming Medical University (Grant Number 202001AY070001-074), Prof. Guo Jun Expert Workstation in Yunnan Province (Grant Number 202105AF150038), the University Key Laboratory of Integrative Melanoma Therapy approved by Education Department of Yunnan Province, the Fundamental Research Project of Yunnan Provincial Department of Science and Technology (202301AT070129), the Joint Special Funds for the Department of Science and Technology of Yunnan Province-Kunming Medical University (Grant Number 202401AY070001-360) and the Yunnan Provincial Department of Education Science Research Fund Project (Grant Number 2023Y0655, 2024Y234). Funded by Yunnan Province Science and Technology Talents and Platform Plan Project (202305AF150067). Yunnan Provincial Department of Science and Technology Key Research and Development Plan for Social Development Special Projects (202403AC100022).

Availability of data and materials

All data generated or analyzed during this study are included in this article and additional data are available from the corresponding author upon reasonable request.

Declarations

Ethics approval and consent to participate

The animal experiment was conducted according to the guidelines set by the Animal Experimental Ethical Committee of Kunming Medical University, and the animal experiment was approved by the Animal Experimental Ethical Committee of Kunming Medical University (approval no. KMMU2021713, Approval date: February 2021).

Consent for publication

All authors have reviewed the final version of the manuscript and approved it for publication.

Competing interests

The authors declare no competing interests.

Received: 14 March 2024 Accepted: 24 May 2024
Published online: 13 June 2024

References

Ahir BK, Engelhard HH, Lakka SS (2020) Tumor development and angiogenesis in adult brain tumor: glioblastoma. Mol Neurobiol 57:2461–2478
Alifieris C, Trafalis DT (2015) Glioblastoma multiforme: pathogenesis and treatment. Pharmacol Therapeut 152:63–82
Alphandéry EJC (2020) Nano-therapies for glioblastoma treatment. Cancer 1(12):242
Carlsson SK, Brothers SP, Wahlestedt C (2014) Emerging treatment strategies for glioblastoma multiforme. EMBO Mol Med 6:1359–1370
Carvalho B, Lopes JM, Silva R, Peixoto J, Leitão D, Soares P, Fernandes AC, Linhares P, Vaz R, Lima J (2021) The role of c-Met and VEGFR2 in glioblastoma resistance to bevacizumab. Sci Rep 1(11):6067
Cattaneo MG, Pola S, Francescato P, Chillemi F, Vicentini LM (2003) Human endostatin-derived synthetic peptides possess potent antiangiogenic properties in vitro and in vivo. Exp Cell Res 2(283):230–236
Cheng F, Guo D (2019a) MET in glioma: signaling pathways and targeted therapies. J Exp Clin Cancer Res 38:1–13
Cheng F, Guo D (2019) MET in glioma: signaling pathways and targeted therapies. J Exp Clin Cancer Res CR 1(38):270
Daudigeos-Dubus E, Le Dret L, Bawa O, Opolon P, Vievard A, Villa I, Bosq J, Vassal G, Geoerger B (2017) Dual inhibition using cabozantinib overcomes HGF/MET signaling mediated resistance to pan-VEGFR inhibition in orthotopic and metastatic neuroblastoma tumors. Int J Oncol 1(50):203–211

Fletcher-Sananikone E, Kanji S, Tomimatsu N, Di Cristofaro LFM, Kollipara RK, Saha D et al (2021) Elimination of radiation-induced senescence in the brain tumor microenvironment attenuates glioblastoma recurrence. Cancer Res 81:5935–5947

Gao X, Jiang P, Zhang Q, Liu Q, Jiang S, Liu L, Guo M, Cheng Q, Zheng J, Yao H (2019a) Peglated-H1/pHGFK1 nanoparticles enhance anti-tumor effects of sorafenib by inhibition of drug-induced autophagy and stemness in renal cell carcinoma. J Exp Clin Cancer Res 1(38):1–15

Gao X, Jiang P, Zhang Q, Liu Q, Jiang S, Liu L, Guo M, Cheng Q, Zheng J, Yao H (2019b) Peglated-H1/pHGFK1 nanoparticles enhance anti-tumor effects of sorafenib by inhibition of drug-induced autophagy and stemness in renal cell carcinoma. J Exp Clin Cancer Res CR 1(38):362

Gatto L, Di Nunno V, Franceschi E, Tosoni A, Bartolini S, Brandes AA (2022) Pharmacotherapeutic treatment of glioblastoma: where are we to date? Drugs 5(82):491–510

Grojean M, Schwarz MA, Schwarz JR, Hassan S, von Holzen U, Zhang C, Schwarz RE, Awasthi N (2021) Targeted dual inhibition of c-Met/VEGFR2 signalling by foretinib improves antitumour effects of nanoparticle paclitaxel in gastric cancer models. J Cell Mol Med 11(25):4950–4961

Hosseini ES, Zeinoddini M, Saeedinia AR, Babaeipour V (2020) Optimization and one-step purification of recombinant V antigen production from Yersinia pestis. Mol Biotechnol 62:177–184

Kim MM, Umemura Y, Leung D (2018) Bevacizumab and glioblastoma: past, present, and future directions. Cancer J 24:180–186

Lamer T, van Belkum MJ, Wijewardane A, Chiorean S, Martin-Visscher LA, Vederas JC (2022) SPI "sandwich": combined SUMO-peptide-Intein expression system and isolation procedure for improved stability and yield of peptides. Protein Sci 5(31):e4316

Li R, Wang H, Liang Q, Chen L, Ren J (2022) Radiotherapy for glioblastoma: clinical issues and nanotechnology strategies. Biomater Sci 4(10):892–908

Liu L, Zong ZM, Liu Q, Jiang SS, Zhang Q, Cen LQ, Gao J, Gao XG, Huang JD, Liu Y, Yao H (2018) A novel galactose-PEG-conjugated biodegradable copolymer is an efficient gene delivery vector for immunotherapy of hepatocellular carcinoma. Biomaterials 184:20–30

Morgan RD, Ferreras C, Peset I, Avizienyte E, Renehan AG, Edmondson RJ et al (2022) c-MET/VEGFR-2 co-localisation impacts on survival following bevacizumab therapy in epithelial ovarian cancer: an exploratory biomarker study of the phase 3 ICON7 trial. BMC Med 1(20):59

Tjin Tham Sjin RM, Satchi-Fainaro R, Birsner AE, Ramanujam VM, Folkman J, Javaherian K (2005) A 27-amino-acid synthetic peptide corresponding to the NH_2-terminal zinc-binding domain of endostatin is responsible for its antitumor activity. Cancer Res 9(65):3656–3663

Tsujimoto A, Uehara H, Yoshida H, Nishio M, Furuta K, Inui T, Matsumoto A, Morita S, Tanaka M, Kojima C (2021a) Different hydration states and passive tumor targeting ability of polyethylene glycol-modified dendrimers with high and low PEG density. Mater Sci Eng C 126:112159

Tsujimoto A, Uehara H, Yoshida H, Nishio M, Furuta K, Inui T, Matsumoto A, Morita S, Tanaka M, Kojima CJMS (2021b) Different hydration states and passive tumor targeting ability of polyethylene glycol-modified dendrimers with high and low PEG density. Mater Sci Eng 126:112159

Van Tellingen O, Yetkin-Arik B, De Gooijer M, Wesseling P, Wurdinger T, De Vries H (2015) Overcoming the blood–brain tumor barrier for effective glioblastoma treatment. Drug Resist Updates 19:1–12

Xie J, Zhang X, Meng D, Li Y, Deng P (2023) Identification of potentially high drug-like VEGFR2/c-Met dual-target type II kinase inhibitors with symmetric skeletons based on structural screening. J Biomol Struct Dynam 42:1249–1267

Yao H, Ng SS, Tucker WO, Man K, Wang X-M, Chow BK, Kung H-F, Tang G-P, Lin MC (2009) The gene transfection efficiency of a folate–PEI600–cyclodextrin nanopolymer. Biomaterials 29(30):5793–5803

Zhang W, Duan R, Zhang J, Cheung WK, Gao X, Zhang R, Zhang Q, Wei M, Wang G, Zhang Q (2018a) H1/pHGFK1 nanoparticles exert anti-tumoural and radiosensitising effects by inhibition of MET in glioblastoma. Br J Cancer 4(118):522–533

Zhang W, Duan R, Zhang J, Cheung WKC, Gao X, Zhang R et al (2018b) H1/pHGFK1 nanoparticles exert anti-tumoural and radiosensitising effects by inhibition of MET in glioblastoma. Br J Cancer 4(118):522–533

Zhang W, Duan R, Zhang J, Cheung WKC, Gao X, Zhang R et al (2018c) H1/pHGFK1 nanoparticles exert anti-tumoural and radiosensitising effects by inhibition of MET in glioblastoma. Br J Cancer 118:522–533

Publisher's Note